Photoluminescence Lifetimes of Quantum Dots

Scott Thalman

A senior thesis submitted to the faculty of
Brigham Young University
in partial fulfillment of the requirements for the degree of

Bachelor of Science

John Colton, Advisor

Department of Physics and Astronomy

Brigham Young University

August 2011

ABSTRACT

Photoluminescence Lifetimes of Quantum Dots

Scott Thalman
Department of Physics and Astronomy
Bachelor of Science

We used time-correlated single photon counting to measure the photoluminescence lifetime of solid InGaAs quantum dots (QDs) as well as colloidal CdSe QDs. The InGaAs QDs were grown using a modified Stranski-Krastanov growth method to encourage the formation of QD chains. These QDs had lifetimes between 0.6 ns and 1 ns indicating the possible formation of QD chains. We also investigated the interaction between ruthenium dye molecules and CdSe QDs in solution.

ACKNOWLEDGMENTS

Contents

List of Figures

Chapter 1

Introduction to Quantum Dots

1.1 Overview

In this thesis I describe photoluminescence lifetime measurements performed on two different sets of quantum dot (QD) samples. These measurements help to characterize the photoluminescence properties of these samples as well as determine their potential use in optical devices. Chapter 1 reviews the properties and applications of quantum dots and other quantum nanostructures. A description of the quantum dot samples used in this study is also found in chapter 1. Chapter 2 describes the experimental technique and important instruments used to measure photoluminescence lifetimes. Our results are presented in chapter 3, along with a comparison to previous studies.

1.2 Quantum Dot Applications

The extensive body of research on quantum dots is due to the breadth of their applications. Solid quantum dots like the InGaAs QDs studied in this experiment are currently used in applications involving infrared laser emission and detection [1, 2]. Particularly important in this area is emission at 1300 nm. This wavelength is important for fiber optic communication applications [3].

1

Wavelength spectra of our InGaAs QD samples have shown emission in this region making these samples potentially useful.

In the visible range, QD light emitting diodes are efficient single wavelength emitters and have even been proposed for use in televisions [4]. The wavelength specificity of QDs has been used to create quantum dot lasers [1, 5]. Because the wavelength of emission is dependent on the size and composition of the QD, lasers can be customized to emit at wavelengths covering most of the visible spectrum and into the infrared.

Cadmium selenide (CdSe) quantum dots have been proposed in solar cell applications to broaden the absorption spectrum and increase efficiency [6]. The CdSe nanoparticle can be associated with the charge carrier of the solar cell in such a way that excited electrons in the QD are transferred to the charge carrier and carried away as current. This transfer of charge increases the efficiency of the cell. Furthermore, dye molecules, such as the ruthenium dye, can cause more wavelengths to be absorbed by the system. The ruthenium dye absorbs a broad spectrum of wavelengths and, when attached to CdSe QDs, can increase the amount of charge transferred to the solar cell.

1.3   Quantum Confinement

In semiconducting materials the molecular orbitals of neighboring atoms in a lattice interact to form two different, nearly-continuous energy bands called the valence band and the conduction band. Electrons typically rest in the states of the valence band. These valence band states are lower in energy than the states of the conduction band. Transitions between neighboring states are not possible in the valence band because all of the neighboring states are occupied. This means that electrons in the valence band are restricted to their current state and we say that they are localized. A gap of disallowed energies called the bandgap lies between the valence band and the

conduction band. Energy introduced to the system, typically by photons, can promote an electron to the conduction band. Because the electron has been promoted to the conduction band, there is a vacant state in the valence band. This vacant state is called a hole. The conduction band consists of many vacant energy states. Therefore, an excited electron can easily transition between these states and we say that it is delocalized. After some time the excited electron will relax into its ground state and release energy. This relaxation is also called recombination because the excited electron is recombined with the hole in the valence band. Relaxation to a lower energy state within the conduction band is mediated by lattice vibrations, which dissipate small amounts of energy. Relaxation from the conduction band to the valence band releases energy in the form of photons.

When promotion and relaxation of electrons is mediated by a photon we call these optical transitions. Thus we refer to optical excitation and optical recombination when electrons absorb and emit light. The process by which photons are emitted by optical recombination is called photoluminescence. The time between excitation and recombination is known as the optical recombination time or photoluminescence lifetime. The time-correlated single photon counting technique described in chapter 2 is used to measure this lifetime.

A vast body of research has been performed on semiconductor nanostructures that restrict the free motion of electrons and holes [5, 7–16]. The restriction of electron motion in one or more spatial directions is called quantum confinement because the confined electrons exhibit quantum effects. For example, in a QD an electron is confined in all three dimensions and must occupy one of a discrete set of energy levels as dictated by the Schrödinger equation. Quantum dots are sometimes referred to as zero-dimensional structures because of their three-dimensional confinement. Confinement in two dimension is called a quantum wire and allows electrons to move only along a straight line. If the electron is confined to a single plane the nanostructure is called a quantum well.

Quantum confinement is achieved by creating a potential barrier in the conduction band. Typ-

ically the potential barrier is established by placing semiconductors with differing bandgaps in close proximity. For example, indium gallium arsenide (InGaAs) has a slightly smaller bandgap than gallium arsenide (GaAs). When these two materials are grown adjacent to each other there is a potential difference in the conduction bands at their border. An electron which has enough energy to occupy the conduction band of InGaAs may not have enough energy to occupy the conduction band of GaAs and is, therefore, restricted to the InGaAs lattice. Figure 1.1 is a representation of the band structure of an InGaAs lattice between two GaAs lattices showing the potential barrier created at the boundaries.
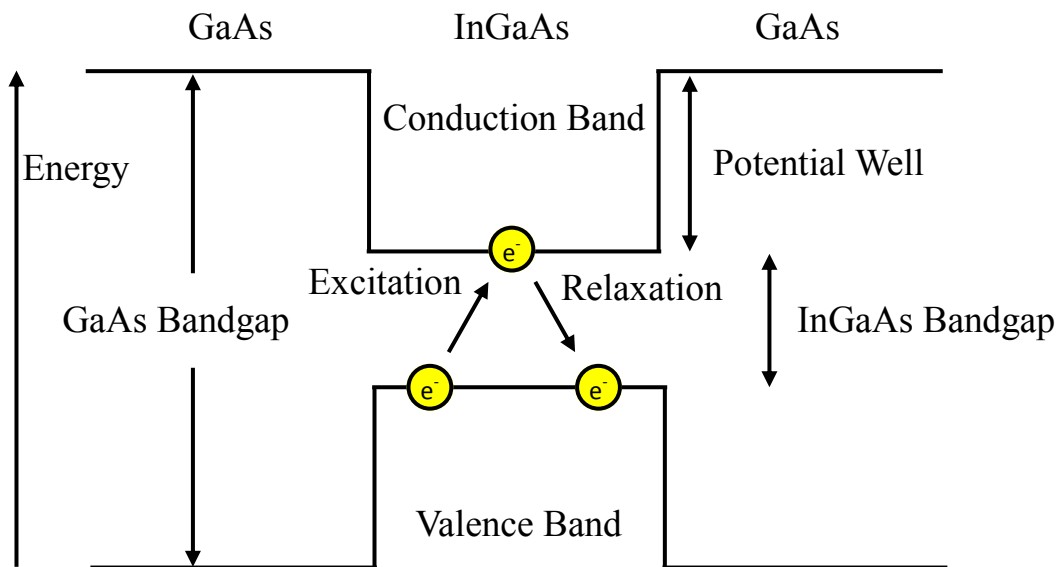

Figure 1.1 The band structure of an InGaAs lattice between two GaAs lattices. Excitation of an electron into the conduction band and relaxation to the valence band are mediated by a photon.

1.4   Quantum Dot Properties

The bound-state solutions to the Schrödinger equation for a particle confined in a potential well represent the allowed wave functions for that particle. Each wave function corresponds to a discrete energy level so the energy of the particle is said to be quantized. This means that an electron confined in a QD is restricted to a discrete set of energy levels. In many ways this is analogous to the quantization of the energy levels of molecular orbitals in an atom. As a result QDs will only emit and absorb light at certain wavelengths matching the energy differences between allowed wave functions. Furthermore, the absorption and emission wavelengths are determined by the size and composition of the QD. Quantum dots can therefore be customized to specific wavelength applications [4].

High intensity excitation can cause QDs to display another quantum effect called the state-filling effect [2]. In the state-filling effect electrons are pumped into excited states faster than they can relax down to their ground states. Because the lower energy excited states are already occupied, newly excited electrons must go into even higher energy excited states. The result is a photoluminescence spectrum that displays multiple peaks corresponding to the multiple excited energy states.

Quantum dots can also be grown in close proximity to one another along a straight line to form a QD chain [14]. Because the potential barrier at the border of the QD is not infinite, the wave functions of confined electrons extend slightly beyond the border of the QD. This means that electrons of adjacent dots can interact. For example, it has been shown that spin information introduced at one end of a QD chain can propagate along the chain through Rabi waves [11, 17].

1.5   Quantum Dot Types

Quantum dots occur in two main types. Quantum dots grown on solid semiconductor wafers represent the first type, which we will call solid QDs. The second type is grown and suspended in liquid solution. These are called colloidal QDs. It should be noted that colloidal QDs are also solid semiconductor crystals and the distinction "solid QD" refers to the medium upon which the dots are grown. In this experiment we measured photoluminescence lifetimes of both types of QD.

The materials used to create QDs are varied, but the most common are III-V and II-VI semiconductors. These names are derived from columns II, III, V, and VI of the periodic table where the elements are found. For example, the III-V materials include combinations of the elements aluminum, gallium, or indium with nitrogen, phosphorus, or arsenic. The solid QDs that we studied were indium gallium arsenide grown on a gallium arsenide substrate. Our colloidal QDs were made of cadmium selenide, which is among the most common of the II-VI materials.

Quantum dots can be created using silicon; however this material has poor optical characteristics compared to the semiconductors described above [18]. Because of silicon's indirect bandgap electrons must change momentum as well as energy in order to be promoted to the conduction band or to relax to the valence band. The change in momentum must be mediated by a phonon and therefore optical transitions are inefficient.

1.6   Quantum Dot Growth Methods

Solid QDs are typically grown using molecular beam epitaxy (MBE) techniques. Molecular beam epitaxy is very effective at depositing monolayers of a desired material on a suitable substrate. This is done in a vacuum by heating the elemental form of the materials to be deposited. Atoms are vaporized and create a beam that can be directed at the substrate. The ratio of each elemental beam, and therefore the ratio of elements deposited, can be precisely controlled through the temperature

of vaporization. This growth method has the advantage that it can produce highly regular samples with very few impurities. Unfortunately MBE is impractical for large scale production of samples because of the long growth times required.

Three main variations of MBE are used to create QDs. In the first method MBE is used to create thin quantum wells by depositing a material with a narrow bandgap, e.g. InGaAs, on a material with a wider bandgap, e.g. GaAs. QDs are formed inside the well when the growth period is periodically interrupted. Interruptions cause monolayer fluctuations in the thickness of the well. Regions that have an extra deposited monolayer have decreased lateral potential. Electrons are weakly confined to those regions while being strongly confined in the overall quantum well. The result is a localized quantum dot.

Quantum dots can also be formed by confining electrons in quantum wells using lithographically attached electrical leads. MBE is used to grow a highly-doped layer on top of the substrate followed by a capping layer of the same material as the substrate Electrons in this doped layer are free to move in two dimensions similar to a quantum well. Photolithography or chemical etching is then used to create metallic leads on top of the capping layer. When a positive voltage is applied to these leads electrons in the doped layer experience a lower potential and congregate near the positively charged lead. This forms a localized QD. In this manner the location of QDs can be precisely controlled, but the lithography techniques are unable to produce QDs smaller than approximately 10 nm in diameter. QDs created using this technique are called lithographically defined QDs.

The final MBE technique is called the Stranski-Krastanov method which forms self-assembled QDs (SAQDs). In this method MBE is used to grow monolayers of a smaller bandgap material on top of a substrate which has a slightly larger lattice constant and a larger bandgap. This difference causes strain in the initial deposition of the smaller bandgap material (called the wetting layer). As more monolayers are added to the wetting layer the strain increases until lattice "buckling" occurs. Buckling causes raised islands of the deposited material to appear. The islands have

a lower potential than their surroundings and therefore act as QDs. Our solid QD samples were grown using a slight modification of the Stranski-Krastanov method. This modified growth method has been shown to form various quantum structures like quantum dashes and QD chains [13].

Colloidal QDs are grown in solution from chemical precursors. Temperature and solvent conditions cause the elements of the desired semiconductor to crystallize. This forms a nanocrystal that can be as small as a few nanometers in diameter. The nanocrystals stay suspended in the solvent to produce a colloid. These nanocrystals act as QDs by confining electrons to their interior.

1.7 Quantum Dot Characterization

The quality of a QD sample is most often determined by its uniformity and optical characteristics. The uniformity of a sample may be determined through microscopy and is not the subject of our experiments. Rather we will focus on one of the optical properties: the photoluminescence lifetime of our samples.

The photoluminescence lifetimes measured in this experiment indicate how long electrons stay in the excited state before relaxing to their ground state and releasing a photon. This information can be used to compare the light emitting efficiency in QDs of different size and composition.

The photoluminescence spectrum is another indicator of the optical quality of a QD sample. The photoluminescence spectra for our solid QDs can be found in Jones et al. [19].

1.8 Samples Studied

Two different types of quantum dot samples were studied in our experiment. Solid InGaAs QDs grown on a gallium arsenide substrate make up the first type. The second type is CdSe colloidal QDs grown and studied in an acetone solution.

The InGaAs QDs were grown using a modified Stranski-Krastanov molecular beam epitaxy

technique (see section 1.6). Dr. Haeyeon Yang of Utah State University developed this technique and our samples were obtained from him. Samples were grown at slightly lower temperatures than typical Stranski-Krastanov growth and then annealed at a higher temperature. Quantum dot formation occurs during the annealing process. The lattice strain relaxes preferentially along the (100) lattice vector causing QDs to form in chains along that vector. For more information about this modified Stranski-Krastanov growth see Kim et al. [13].

The three samples were selected from a series of 10 samples because of prominent, narrow emission peaks near 980 nm. All of the samples in the series, including the three we studied, were grown with different growth parameters.

The CdSe QD samples were grown by a student of Dr. Roger Harrison from the Brigham Young University Department of Chemistry and Biochemistry. The CdSe QDs were suspended in an acetone solution which was then placed in a quartz cuvette for study.

Chapter 2

Time-Correlated Single Photon Counting

2.1 Overview

In this chapter I describe the measurement technique we used to obtain our data. Two instruments are commonly used to obtain time resolved photoluminescence measurements: streak cameras which use time-dependent deflection to create a spatially varying signal, and time-correlated single photon counting (TCSPC) modules. Our measurements were taken using the latter method.

In TCPSC, single photon events at the detector are timed relative to a reference pulse. The sample is excited by a pulsed laser source and as excited electrons relax to their ground state the sample begins to photoluminesce. At the same time the TCSPC module receives a reference signal from a detector in a secondary beam path which starts an internal timer. The photoluminescence is collected and filtered down until no more than one photon per excitation pulse arrives at the detector. The detector produces a voltage pulse in response to the photon, and this photon stops the timer. The time between the excitation pulse and the emission pulse is then recorded. This is repeated for millions of photons and a histogram is created showing the correlation between the number of photons, which is proportional to the photoluminescence intensity, and the time after

excitation.

The electronics in a typical TCSPC card are capable of resolution better than 100 ps. Furthermore, by filtering down the photoluminescence and averaging millions of single photon events, we can achieve signal-to-noise ratios better than 1000:1.

2.2   Experimental Schematics

The solid QDs and the colloidal QDs required slightly different experimental setups. Figure 2.1 shows the schematic for the solid QD TCSPC experiment and Fig 2.2 shows the colloidal QD schematic. The solid QD setup used an 800 nm pulsed titanium:sapphire (Ti:Sapph) laser to excite the samples, an avalanche photodiode (APD) inside the laser cavity itself to detect the reference pulse, and a silicon avalanche photodiode (Si APD) to detect emitted photons. Two high pass wavelength filters combined with the natural cut-off wavelength of the Si APD eliminated emission outside the region of interest. The InGaAs QD samples were mounted in a closed-cycle helium cryostat in order to take measurements at 4 K. The colloidal QD setup used the Ti:Sapph laser with an LBO nonlinear crystal to produce 400 nm excitation, the internal APD to detect the reference pulse, a photomultiplier tube (PMT) to detect emission, and a monochromator to select the wavelength of interest. The pulse generator was used in the CdSe QD experiments because of limitations with the TCSPC card. Refer to section 2.6 and appendix A.1.1 for more information regarding the pulse generator. Measurements for the CdSe QDs were taken at room temperature (300 K).

In the next few sections I will describe the functions of the major instruments used in our setup. The settings of individual instruments, especially the TCSPC modules, can be found in appendix A.

Figure 2.1 Experimental schematic of the InGaAs quantum dot TCSPC measurement. Main components include the pulsed laser, cryostat, Si APD, laser's internal APD, and the Ortec Model 9353 TCSPC module. See appendix A.2 for settings used in this experiment.
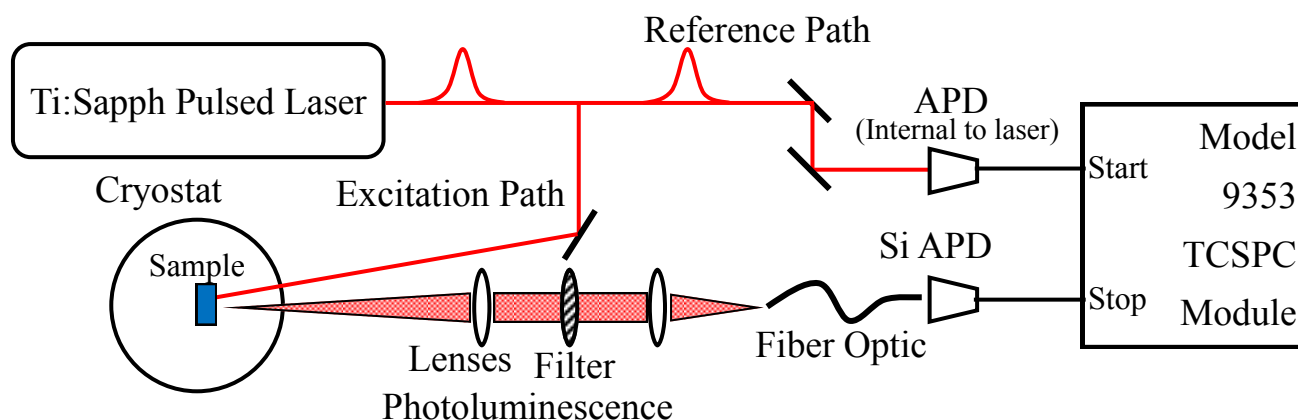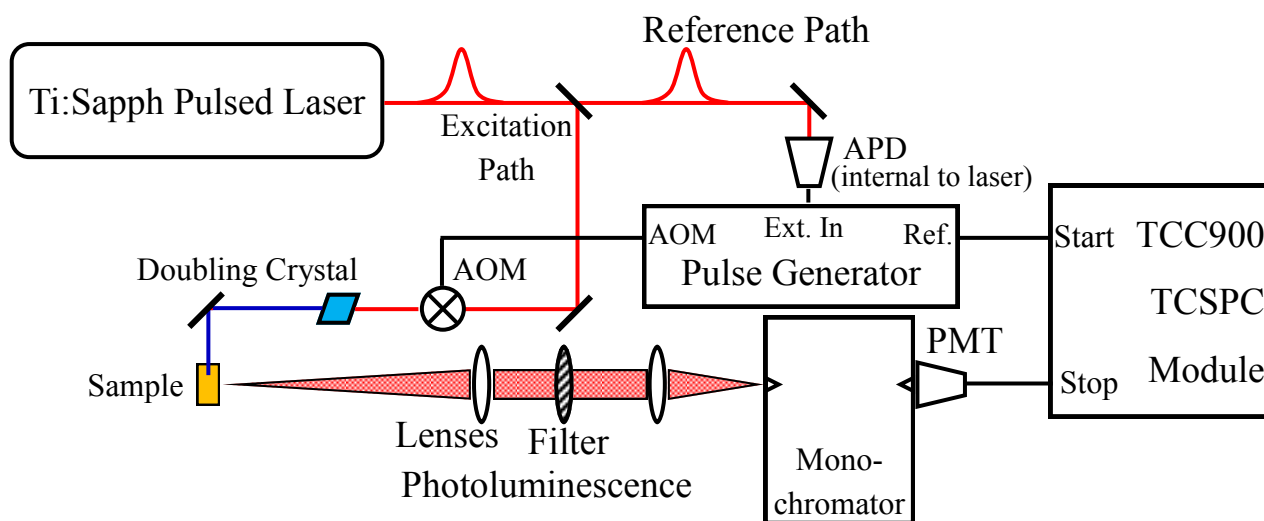

Figure 2.2 Experimental schematic of the CdSe quantum dot TCSPC measurement. Main components include the pulsed laser, AOM, frequency doubling crystal, PMT, photodiode, and the TCC900 TCSPC module. See appendix A for information about the pulse generator and experimental settings.

2.3   Pulsed Ti:Sapph Laser

The pulsed laser is a key component of the experimental setup as it both excites the sample and provides a very precise time reference. We used a home-built, optically pumped Ti:Sapph laser to generate approximately 30 fs pulses at a repetition rate of 82 MHz. Because the 30 fs pulses were five orders of magnitude shorter than the expected photoluminescence lifetime of our sample, we were able to assume instantaneous excitation. In other words, electrons in the sample can be pumped into excited states instantly and the measurement of the photon emission over time can be referenced to that instant.

Our laser uses Kerr lens modelocking to achieve short pulses. The Ti:Sapph crystal is optically pumped using a Spectra Physics 532 nm pump laser and produces red laser light with a tunable wavelength range of 700-1000 nm. The laser will operate in continuous wave (CW) mode and is tuned to a state that hops rapidly between two widely separated modes. We have found that this metastable state is most favorable for modelocking our laser. Tapping one of the end mirrors of the laser cavity creates a nonuniform intensity perturbation. A nonlinear optical effect called the Kerr effect causes high intensity light to be focused as it passes through the crystal while low intensity light is not. Thus high intensity portions of the perturbation are amplified creating a pulse. Only the laser modes that are in phase with the pulse will be amplified. Thus when the laser is operating in pulsed mode we say that it is modelocked. With each pass through the crystal the pulse is amplified more and the CW contribution rapidly becomes negligible. The precise internal dimensions of the laser cavity determine the repetition rate of the pulses (82 MHz for our laser).

Modelocking and pulse width are monitored by analyzing the spectrum of the beam. A reflected beam in the cavity is diffracted off of a grating onto a real time CCD. The output of the CCD is attached to a monitor for observation. When the laser is operating in CW mode only one narrow band is observed on the screen. The metastable state is identified by multiple narrow bands or "mode hopping" where the laser rapidly alternates between two bands widely separated in

wavelength. When modelocking occurs after introducing a perturbation, the narrow band changes to a broad spectrum. From the Heisenberg uncertainty principle a broad frequency spectrum indicates a narrow temporal distribution, or a short pulse. The pulse width can be calculated from the frequency spectrum using the uncertainty principle.

The InGaAs QDs were excited by a 9 mW beam that was first unfocused and then focused on the sample. Because the CdSe experimental setup required use of a frequency doubling crystal, the excitation power of the CdSe QDs was decreased. The excitation power was maximized by eye, but never measured.

2.4   Collecting Optics

When excited electrons in the sample relax and emit photons, they do so in random directions. As a result the photoluminescence must be collected and focused into the detector. This is done using two lenses to collimate the photoluminescence and then focus it onto the detector or monochromator.

Because the TCSPC module creates a statistical representation of the luminescence decay, the photoluminescence must be filtered down so that each excitation pulse produces a maximum of one photon at the detector. If a single excitation were to produce multiple photons, only the earliest photon would register a time point on the histogram. The result would be a histogram that is biased to early photons and would not accurately represent the decay. The TCSPC module monitored the counts per second at the detector and filters were added until the counts per second were 100 to 1000 times lower than the repetition rate of the laser. This ensured that two photon events were unlikely.

In the solid QD experiment, two chromatic filters were used. A high-pass 900 nm filter and a high pass 850 nm filter were placed in front of the detector to prevent the detection of stray laser

light and focus on the main emission peak at 980 nm. Emission beyond 1000 nm was excluded from measurement by the natural cut-off wavelength of the Si APD.

In the colloidal QD experiment a monochromator was used to select the peak emission wavelength of 557 nm.

2.5   Single Photon Detectors

The two different types of QD samples required different detectors. The infrared emission of the solid QD posed a particular problem. The detectors we had available were either insensitive to infrared wavelengths or unable to detect single photons. As a result we resorted to a silicon avalanche photodiode whose efficiency was reduced greatly beyond 1000 nm. Even though we were not be able to study the entire spectral range of our samples, we were still able to detect emission at the primary peak wavelength of 980 nm.

For the colloidal QDs the emission wavelengths were in the visible range. This meant a low voltage photomultiplier tube could be used to detect photon events.

2.6   TCSPC Modules

The TCSPC module is the most important element of the experimental setup. The goal of the module is to determine the time between the "start signal" and the "stop signal." In photoluminescence lifetime measurements, the start and stop signals are produced by the single photon detectors and the time between them corresponds to the optical recombination time. The fast electronics contained in the TCSPC card allow accurate time resolution.

Because one of our TCSPC modules was incompatible with our Si APD detector, two different TCSPC modules were used in our experiments. For the solid QD measurements, which used the Si APD, we used an Ortec Model 9353 fast digitizer borrowed from Dr. Michael Ware of Brigham

Young University. For the colloidal QD measurements we used an Edinburgh Instruments TCC900 TCSPC card. The settings used for each of the two experiments can be found in appendix A.

2.6.1   Ortec Model 9353 Fast Digitizer

The Ortec Model 9353 fast digitizer is the simpler of the two TCSCP modules we used. It uses a 10 GHz internal clock to produce a time stamp for each pulse and compares the time stamps of the start and stop signals. This mode of operation is referred to as "time of flight mode" (TOF). In TOF mode, the Model 9353 can produce up to 100 ps time resolution. This resolution is not as high as the Edinburgh Instruments TCSPC card, however, the Edinburgh Instruments TCC900 required a negative voltage pulse from the detector. The Si APD produced positive voltage peaks in response to emitted photons and therefore could not be used to trigger the TCC900 card. The Ortec Model 9353 could be triggered by either positive or negative peaks and was therefore used in the InGaAs QD measurements.

2.6.2   Edinburgh Instruments TCC900

The Edinburgh Instruments TCC900 TCSPC card uses a more complicated system of electronics to obtain more accurate time resolution. This card was able to achieve a maximum resolution of 1 ps. This increase in resolution is possible because of the three main components of the TCC900; the constant fraction discriminator (CFD), the time to amplitude converter (TAC), and the analog to digital converter (ADC).

Like the Ortec Model 9353, the TCC900 is triggered with a start pulse and a stop pulse from the photon detectors. The signals first pass the CFD which replaces the more typical threshold trigger. In many other systems, including the Ortec fast digitizer, a pulse is detected when the voltage reaches a certain threshold level. This method can introduce a small amount of error, called "time walk" in the timing of the trigger if the pulses do not have a uniform amplitude (see Fig. 2.3). For
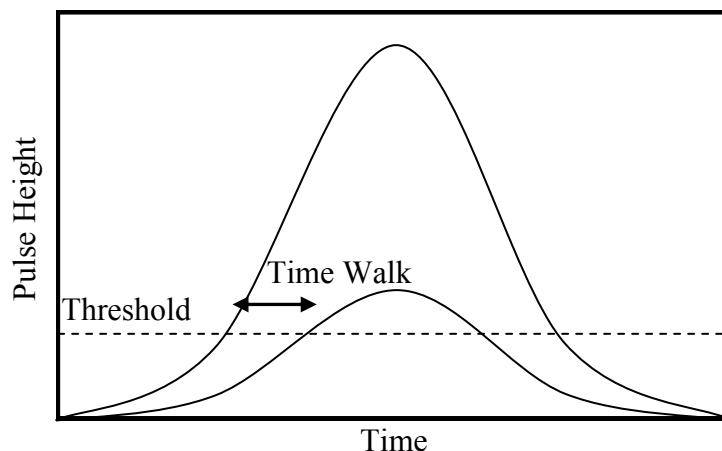
Figure 2.3 This figure shows the inherent temporal uncertainty of threshold triggers. The peaks of both pulses arrive at the same time, but the pulse with a larger amplitude reaches the threshold faster than the small pulse. This phenomenon is known as "time walk."

example, a large peak will reach the threshold slightly faster than small peak and therefore trigger slightly sooner. A CFD, on the other hand, accounts for variations in amplitude by triggering once the pulse has reached a certain fraction of its amplitude. Because the pulse shape is the same for each pulse, even if the amplitude varies, the time to reach this fractional threshold will be the same. The result is more precise definition of when the pulse occurred.

Once the CFD of the start signal path has been triggered, the time to amplitude converter begins measuring the time until the "stop" signal is received. Triggering the TAC begins the charging of a capacitor. Because of the well-defined relationship of charge on a capacitor vs. time, this can be used to accurately measure the time between signals. For photoluminescence lifetime measurements, the time between signals corresponds to the time between excitation and recombination.

When a pulse is received at the "stop" input the charge on the TAC is measured and passed to the analog to digital converter. The ADC uses the time dependence of the capacitor to determine the recombination time of the detected photon. The ADC resolves the measurement time into very small time intervals. The detected photon is counted in the interval corresponding to

its measured recombination time. The software of the TCSPC card can then create a histogram displaying the number of photons counted in each interval vs. that interval's corresponding time after excitation. Because the intensity is proportional to the number of photons this equates to a plot of photoluminescence intensity over time.

2.7 Cryostat

The photoluminescence of the solid QDs is typically dependent on their temperature. The photoluminescence spectra of the samples used in this study showed strong temperature dependence (ref. Jones et al. [19]). For this reason the solid QDs were mounted to the cold finger of a Cryo Industries closed-cycle helium cryostat. Exterior windows allowed optical access to the samples through which we excited them and collected photoluminescence. Samples were measured at 4 K.

2.8 CdSe QD Specific Equipment

The CdSe QDs required excitation at a wavelength below 500 nm. The laser pulses from our Ti:Sapph laser were centered at 800 nm so a frequency-doubling, nonlinear crystal was used to produce excitation at 400 nm.

The photoluminescence lifetimes of the colloidal QDs were much longer than the repetition rate of the laser. This meant that the photoluminescence did not decay back to baseline levels before the arrival of the next excitation pulse. The peaks would simply build upon each other so that only the early part of the decay curve was distinguishable while the latter part was hidden by subsequent peaks.

In order to observe the latter end of the photoluminescence decay we added an acousto-optic modulator (AOM) to the excitation beam. The AOM acted as a fast shutter to block pulses and allow the photoluminescence to decay fully. However, the AOM was not fast enough to allow one

pulse through at a time. The functional limit of the AOM was about 100 ns which corresponds to 5-6 excitation pulses. The duty cycle of the AOM could be adjusted to allow the last excitation to fully decay before the next series of pulses, allowing us to measure the photoluminescence lifetime of the last pulse.

2.9   Impulse Response Function

Previous lifetime measurements of InGaAs QDs [8] led us to expect lifetimes on the order of one nanosecond. We knew this would approach the limits of our Si APD so we decided to measure the instrument's response to scattered laser light. The pulse width of the laser was 30 fs which is five orders of magnitude shorter than the expected lifetimes. This gave us an adequate approximation to a delta function in order to measure the impulse response function (IRF) of our detector.

The laser light was focused onto a portion of the sample area that was not covered by a sample. Scattered light was collected and focused into the detector as described above, and a lifetime measurement was taken. The result was a luminescence decay curve similar in shape to our sample measurements. The lifetime of that curve represented our instrument response time and was determined to be about 1 ns. The measured data for our InGaAs QD samples was only slightly longer than this, with lifetimes of approximately 1.7 ns.

We concluded that our measured data must be a convolution of the impulse response function with the real photoluminescence lifetime. In order to determine the true photoluminescence lifetime of our samples we would need to perform a deconvolution on each data set. The results of our deconvolution calculations are in section 3.2.

Chapter 3

Results and Discussion

3.1 Expected Results

Previous studies have shown that InGaAs QDs grown on GaAs substrates have photoluminescence lifetimes of about 1 ns [8]. Other QD structures including QD chains and QDs grown in close proximity to quantum wells have shown that the photoluminescence lifetimes are lengthened in these structures [20]. In order for recombination to occur the excited electron must interact with the hole in the valence band. In highly confined structures, like quantum dots, this happens quickly. In coupled systems the electrons and holes can move farther apart and therefore recombination times are lengthened.

The modified Stranski-Krastanov growth method used to grow our InGaAs QDs has been shown to create QD chains [13]. We, therefore, were expecting to measure lifetimes slightly longer than the previously published lifetimes for isolated QDs.

For our colloidal QD samples we expected exponential decay curves with lifetimes of between 5 ns and 25 ns.

3.2   Deconvolution

After comparing the measurements performed on our solid QD samples to the impulse response function of our Si APD detector, we concluded that deconvolution would be necessary to determine the actual value of the photoluminescence lifetimes. Using this technique we were able to measure short lifetimes between 0.6 ns and 1 ns for our InGaAs QDs even though our impulse response was as large as 1 ns.

The measurements we took were a convolution of the real photoluminescence decay with the impulse response function (IRF). The similarity of the measured lifetimes to the IRF meant that the convolution was non-negligible. In order to accurately determine the real photoluminescence lifetime we would have to deconvolve the two. The convolution theorem shown in Eqn. 3.1 indicates that analysis of the data can be done by taking the Fourier transform of the data.

$$\mathscr{F}[h] = \mathscr{F}[f \otimes g] = \mathscr{F}[f] \times \mathscr{F}[g] \tag{3.1}$$

In this equation h represents the data that we measured, f represents the real photoluminescence decay, g is the impulse response function, $\mathscr{F}$ indicates the Fourier transform, and $f \otimes g$ represents the convolution of f with g. In Fourier space the measured data, which is a convolution of the real measurement with the IRF, is a product of the two. The measured data can then be divided by the IRF and the inverse Fourier transform calculated to deconvolve the real decay as shown in Eqn. 3.2 (where $\mathscr{F}^{-1}$ indicates the inverse Fourier transform).

$$f = \mathscr{F}^{-1}\left[\frac{\mathscr{F}[h]}{\mathscr{F}[g]}\right] \tag{3.2}$$

As shown in Fig. 3.1 our solid QD data was a series of peaks and decays coinciding with the 82 MHz repetition rate of our pulsed laser. For each sample and experimental parameter one of those peaks was chosen to be used in the analysis. Note the uniformity of the peaks in Fig. 3.1, so this
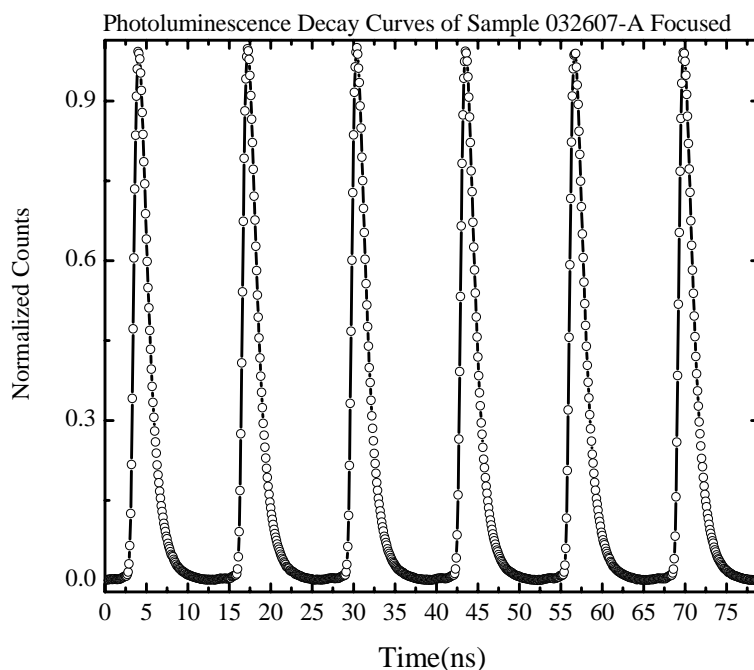
Figure 3.1 The measured data for sample 032607-A under focused excitation before deconvolution. The data displays a series of peaks corresponding to the instantaneous excitation followed by a fast exponential decay.

choice of a representative peak is acceptable. Similarly one peak was chosen as the representative IRF.

The deconvolution calculations were performed in Matlab on the representative peak from each measurement. In order to perform the deconvolutions, the baseline counts were subtracted from the data and zeros were added to ensure an even number of points on each side of the peak. The Matlab code performed the Fourier transform, division of the IRF, and then the inverse Fourier transform. The deconvolved measurements were then plotted and fitted with an exponential curve to yield the final photoluminescence lifetime. A representative photoluminescence decay with the impulse response function and an expenential fit is shown in Fig. 3.2

Because the CdSe QD measurements used a faster instrument and the photoluminescence life-
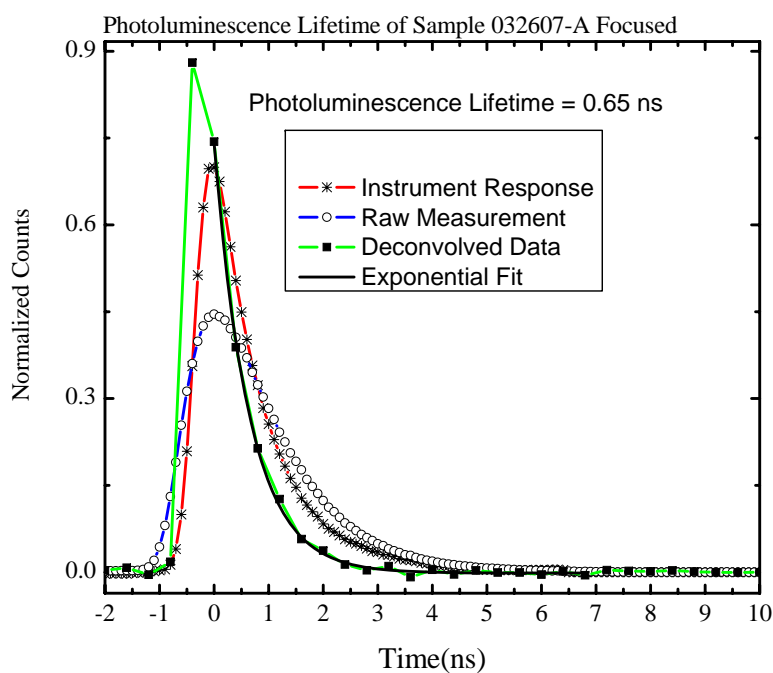
Figure 3.2 A representative photoluminescence decay from sample 032607-A. The measured data (indicated by open circles) is shown along with the impulse response (asterisks) and the final deconvolved data (filled squares). The exponential regression is plotted over the deconvolved data and has a lifetime of 0.65 ns.

times were longer, the deconvolution technique was not needed.

3.3   InGaAs Quantum Dots

Samples were named according to the date on which they were grown with A or B indicating the first or second sample grown that day. Thus sample 032607-A was the first of two samples grown March 26, 2007. These samples were excited by a 9 mW beam that was first unfocused and then focused on the sample. A summary of all of the InGaAs QD photoluminescence lifetimes is found in Table 3.1.

Sample	Unfocused Lifetime	Focused Lifetime
032607-A	0.78 ns	0.65 ns
032607-B	0.86 ns	0.78 ns
032907	0.96 ns	0.60 ns

Table 3.1 Summary table of the photoluminescence lifetimes for the InGaAs QD samples.

3.3.1   Sample 032607 A

Photoluminescence spectra for sample 032607-A indicate the successful creation of QDs, with photoluminescence peaks at 980 nm and 1350 nm. Photoluminescence lifetime measurements were restricted to the 980 nm peak. With low intensity excitation this sample had a measured photoluminescence lifetime of 0.78 ns. When the laser was focused, giving higher excitation intensity, the photoluminescence lifetime was faster at 0.65 ns. The deconvolved decays along with exponential fits are shown in Figs. 3.3 and 3.4.
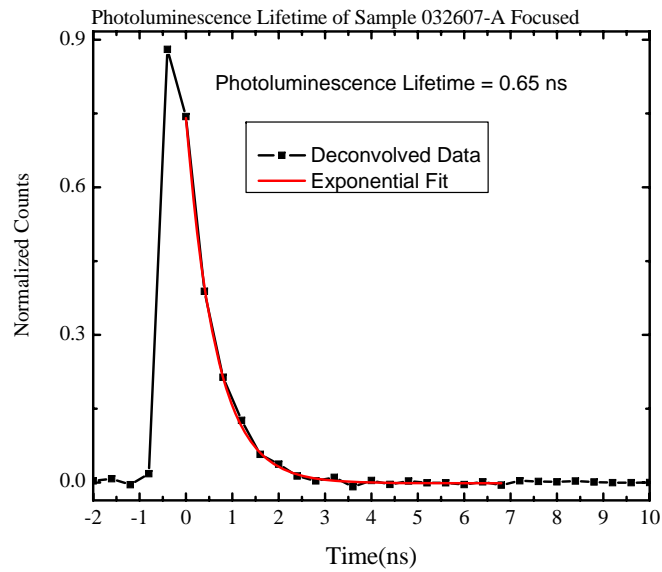
Figure 3.3 Photoluminescence decay of sample 032607-A with a focused excitation beam. The photoluminescence lifetime is 0.65 ns.
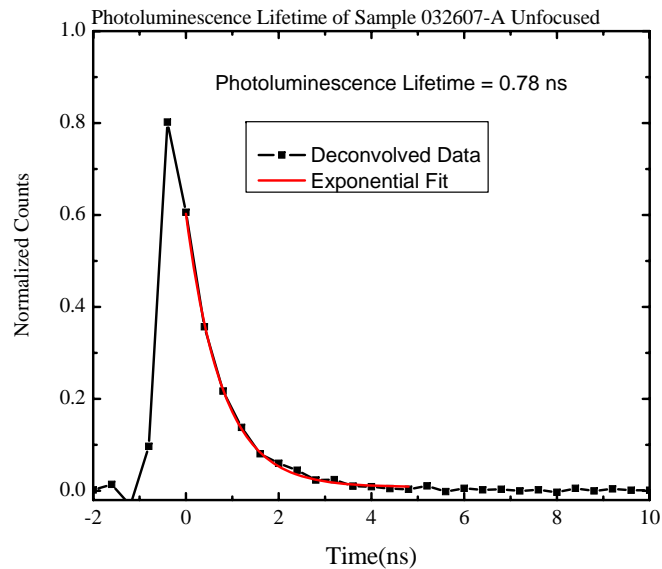

Figure 3.4 Photoluminescence decay of sample 032607-A with an unfocused excitation beam. The photoluminescence lifetime is 0.78 ns.

3.3.2 Sample 032607 B

Sample 032607-B had photoluminescence peaks that were slightly broader than the two other unmodulated solid QD samples we studied. The broadness of the peaks is most likely an indication of nonuniformity in the sizes of the QDs. The photoluminescence lifetimes for this sample were slightly longer than those of sample 032607-A. The high intensity lifetime was 0.78 ns and the unfocused beam 0.86 ns. Photoluminescence decay curves for this sample are shown in Figs. 3.5 and 3.6.
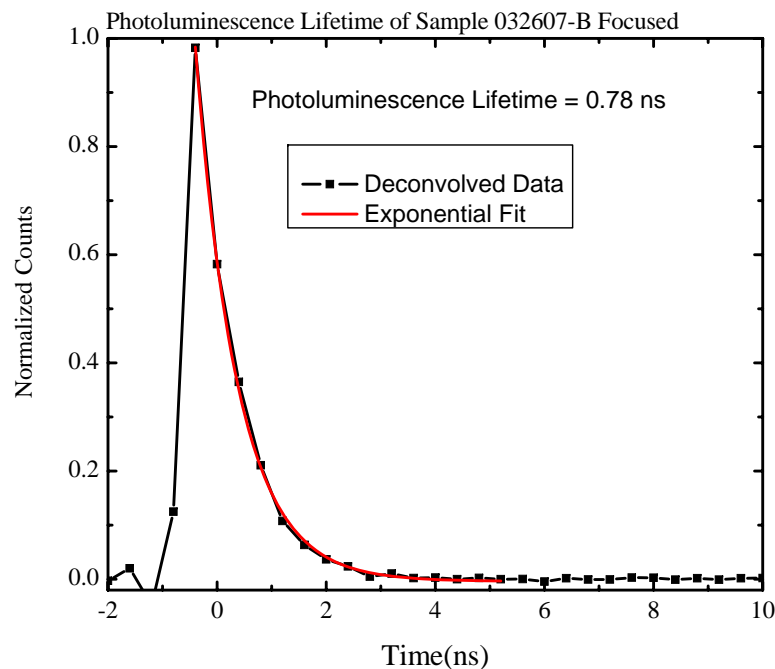

Figure 3.5 Photoluminescence decay of sample 032607-B with a focused excitation beam. The photoluminescence lifetime is 0.78 ns.
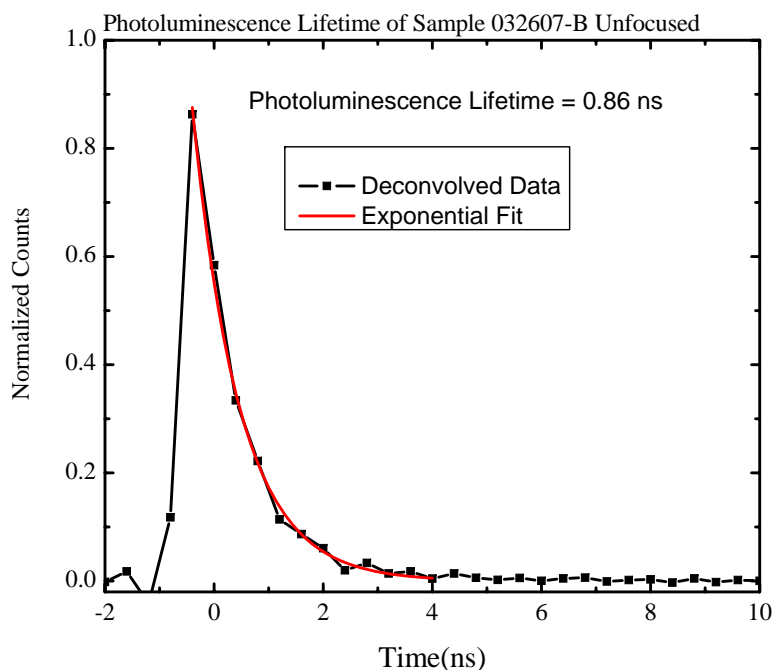
Photoluminescence Lifetime of Sample 032607-B Unfocused

Photoluminescence Lifetime = 0.86 ns

Figure 3.6 Photoluminescence decay of sample 032607-B with an unfocused excitation beam. The photoluminescence lifetime is 0.86 ns.

3.3.3 Sample 032907

This sample was grown under the same parameters as sample 032607-A but annealed at a slightly higher temperature. The photoluminescence spectra were much less sensitive to temperature and excitation intensity with this sample than the other unmodulated samples. The photoluminescence lifetimes, however, were were much more dependent on intensity than the other samples. This sample had a photoluminescence lifetime of 0.96 ns when the excitation beam was unfocused, but the lifetime shortened to 0.60 ns when the beam was focused. Photoluminescence decay curves for this sample are shown in Figs. 3.7 and 3.8.
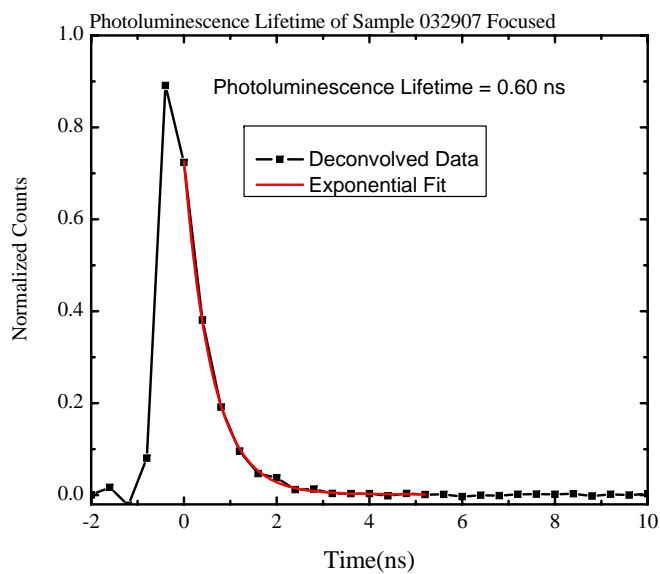
Figure 3.7 Photoluminescence decay of sample 032907 with a focused excitation beam. The photoluminescence lifetime is 0.60 ns.
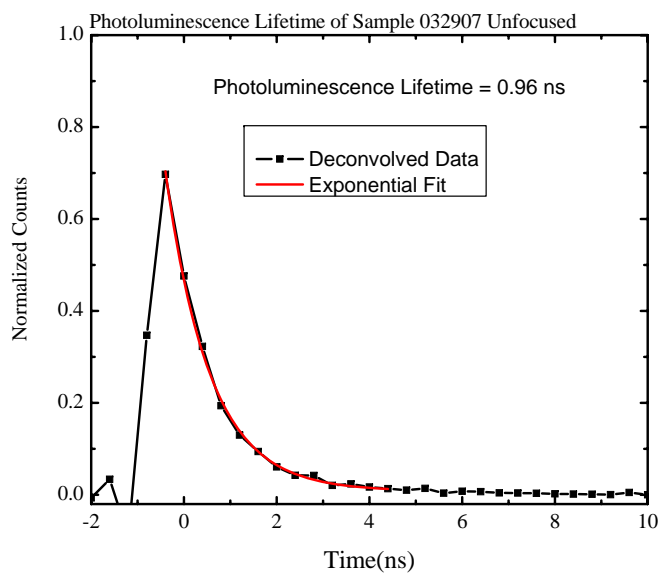

Figure 3.8 Photoluminescence decay of sample 032907 with an unfocused excitation beam. The photoluminescence lifetime is 0.96 ns.

3.4   CdSe Quantum Dots

The colloidal samples measured exhibited multiple exponential decays, typically a fast decay followed by a slower one. In order to study this we performed high resolution short lifetime measurements as well as lower resolution longer lifetime measurements. The limitations of our AOM prevented us from reducing the duty cycle of the excitation to a single pulse. As a result the later portion of the photoluminescence decay was observed by allowing a series of 4-5 pulses to excite the sample and then observing the decay after the final pulse. The short measurements were performed by analyzing only the first few nanoseconds of the decay. Because the repetition rate of the pulsed laser was much faster than the decay time of the sample, the photoluminescence could not fully decay before the next excitation. Enough decay had occurred, however, to allow analysis of the early part of the decay curve.

Figure 3.9 demonstrates the fast and slow decay curves of the CdSe sample. In this figure a series of 8 pulses is allowed to excite the sample followed by a long decay period. The fast lifetime can be determined by fitting an exponential curve to one of the early peaks. This yielded a lifetime of 7 ns. To find the slow photoluminesence lifetime we focused on the late portion of the last peak. An exponential fit of this region showed that the slow lifetime was 23 ns. The exponential fits for these regions can be seen in Fig. 3.9.

3.5   Future Studies

Each of the solid QD samples displayed faster photoluminescence lifetimes when the intensity was increased. This indicates the potential for future studies investigating the intensity dependence of the photoluminescence lifetime. In addition, our detector limited the wavelengths that we were able to study. Further studies could include lifetime measurements at many different wavelengths, though wavelengths beyond 1000 nm would require a different detector.
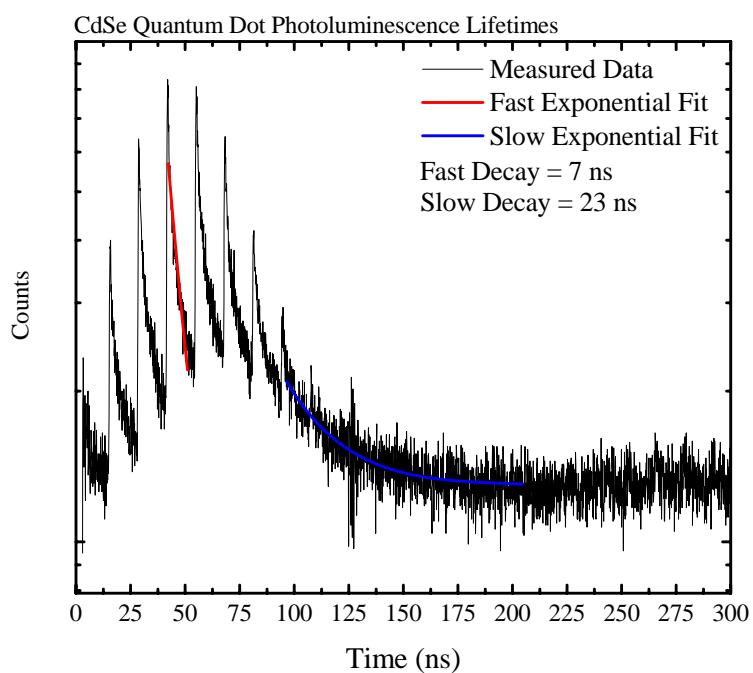
Figure 3.9 Photoluminescence decay of the CdSe QD sample. The AOM allows a series of 8 pulses to excite the sample which produces to overall rise early in the measurement. An exponential fit of the fast, 7 ns decay of one of the excitation pulses is shown along with a fit of the slow, 23 ns decay of the last pulse.

The cryostat used for the solid QD measurements is capacle of controlling temperatures between 4 K and 300 K. Therefore, future studies could also include photoluminescence lifetime measurement at various temperatures.

Finally, the collaborator who grew our current InGaAs QD samples, Dr. Yang, has grown a new, laser-modulated InGaAs QD sample. A laser diffraction pattern was used to heat some areas of the gallium arsenide substrate during epitaxial growth. Since the formation of QDs is highly dependent on the temperature during growth, QDs were preferentially formed in the destructive interference fringes of the diffraction pattern where no heating occurred. As a result, alternating areas of high and low QD density are apparent on the surface of the sample. Preliminary photoluminescence spectra of this sample have already been measured, and lifetime measurements will follow.

Appendix A

TCSPC Module Parameters

A.1 Edinburgh Instruments TCC900

A.1.1 Pulse Generator

The Edinburgh Instruments TCC900 module required creative use of an Agilent 8110A pulse generator to generate a suitable stream of reference pulses. Our pulsed Ti:Sapph laser operated at a repetition rate of 82 MHz. The laser pulses were detected by an avalanche photodiode internal to the laser cavity which produced positive amplitude pulses. These two characteristics were incompatible with the TCC900 card, which required negative pulses and a repetition rate below 10 MHz. The pulse generator was used to reduce the repetition rate of the reference stream and invert the output amplitude. It was also used to trigger the AOM responsible for creating packets of optical pulses to excite the sample.

The pulse generator was operated in "triggered pulses" mode with the output of the photodiode connected to the external trigger. The channel 1 output was set to an appropriate level for the TCC900. This was done using a high voltage of 0 V and a low voltage of -0.6 V. The delay and pulse width were then adjusted to, respectively, reduce the repetition rate and center the
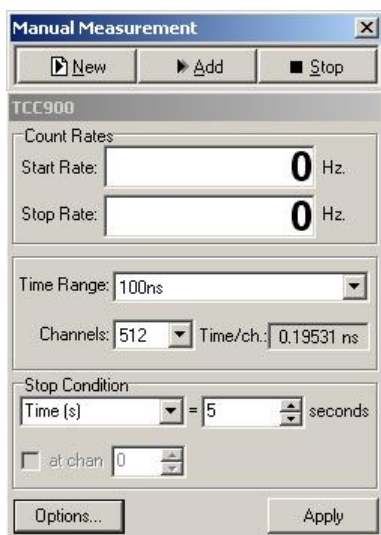
measurement on the measurement window.

A.1.2   Measurement Window

Both the TCC900 and the Ortec Model 9353 took measurements inside a predetermined measurement window. In other words, a time range had to be selected before each measurement. That range was then divided into bins which determined the resolution of the measurement. For the TCC900 the time range and number of channels were selected in the "Manual Measurement" dialog box (see Fig. A.1(a)). The CdSe QD measurements were taken with windows of 50 ns, 200 ns, and 500 ns. The number of channels used varied between 512 and 4096. The resolution was determined by dividing the time window by the number of channels used. For example, a 50 ns scan with 1024 channels corresponds to a time resolution of 49 ps/point. Occasionally, a bug in the time settings would cause a mismatch between the data and the time scale. When this occurred the photoluminescence peaks were compressed together. Changing time scales was typically sufficient to alleviate the error.

The beginning of the measurement window is determined by the reference pulse. Extra delays that were a result of differences in the cable lengths and the optical path lengths often caused the excitation and luminescence decay curves to be shifted temporally relative to the reference pulse. When this happened, the region of interest was not entirely visible in the measurement window. The "Delay" parameter found in the "Time Range Settings" tab of the "TCC900 Options" dialog box (see Fig. A.1(c)) is designed to compensate for this effect, but we had little success in using it consistently. Instead, pulse generator settings were used to adjust the measurement temporally.

With the pulse generator triggered by the laser through the internal APD, both channels were set to the same delay in order to fix the overall repetition period of our experiment.. Our measurements were typically performed with a delay setting of 300 ns, corresponding to a repetition rate of 3.3 MHz. This means the TCC900 would receive reference signals at a rate of 3.3 MHz instead of 82
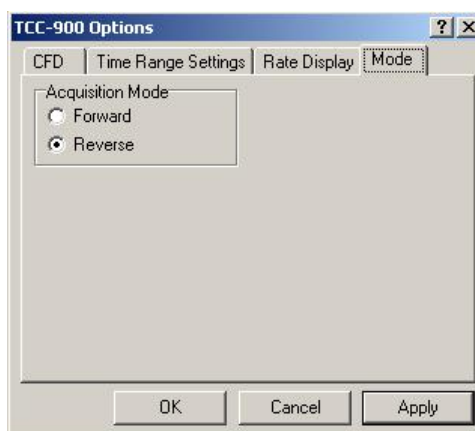
(a) Manual Measurements
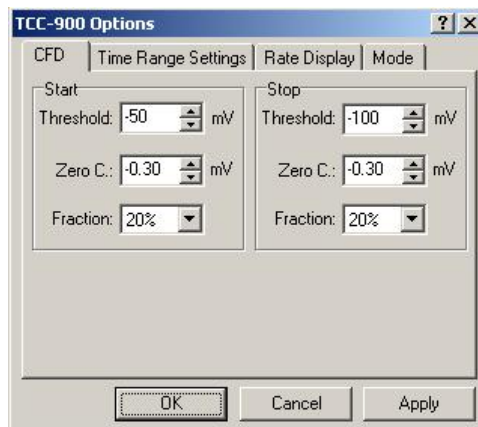
(b) Options: CFD
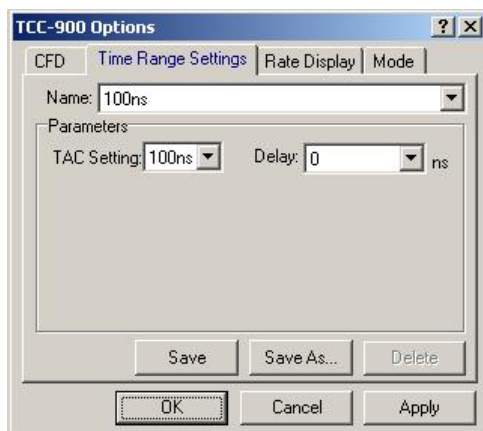
(c) Options: Time Range Settings

(d) Options: Mode

Figure A.1 Important dialog windows for the Edinburgh Instruments TCC900

MHz, which was necessary due to the cards's 10 MHz limitation. Triggers that occurred during the 300 ns delay were ignored by the pulse generator, so the overall repetition rate was not interrupted. The AOM was controlled at this same rate producing one packet of excitation pulses every 300 ns.

The width of the reference pulses was then adjusted so that the excitation packet arrived sooner or later relative to the reference pulse. In this way we could shift the excitation packet and the

decay curves to the left or right of the measurement window in order to measure the entire region of interest.

A.1.3   Forward and Reverse Modes

The TCC900 can operate in either forward or reverse mode. Switching between these two modes can be done in the "Mode" tab of the "TCC900 Options" dialog box (see Fig. A.1(d)). The forward mode is simpler and operates as described in section 2.1. Operating this way the reference pulses must be connected to the "Start" input of the TCC900 and the photoluminescence signal must be connected to the "Stop" input.

The reverse mode does the opposite, using the photoluminescence to trigger the start pulses and the reference pulses to create stop signals. A predetermined, constant delay follows each reference pulse. When the photoluminescence creates a start pulse, the TAC measures the time until the end of the delay. By subtracting the measured time from the constant delay time, the photon's arrival time can be deduced.The software provided with the TCC900 automatically adjusts the data so that the times reported in reverse mode reflect the time after excitation and not the time until the next stop signal. Because the photoluminescence is filtered down so that only 1 in 1000 excitations produce a photon at the detector, reverse mode has the advantage that the time to amplitude converter is only activated when there is a start pulse. By eliminating the need for the TAC to reset every cycle, the maximum number of counts processed can be increased by as much as a factor of 20. This translates to higher repetition rates and faster scan times. For this reason our CdSe QD measurements were typically performed in reverse mode. Figure A.2 shows the difference between forward and reverse modes of operation.
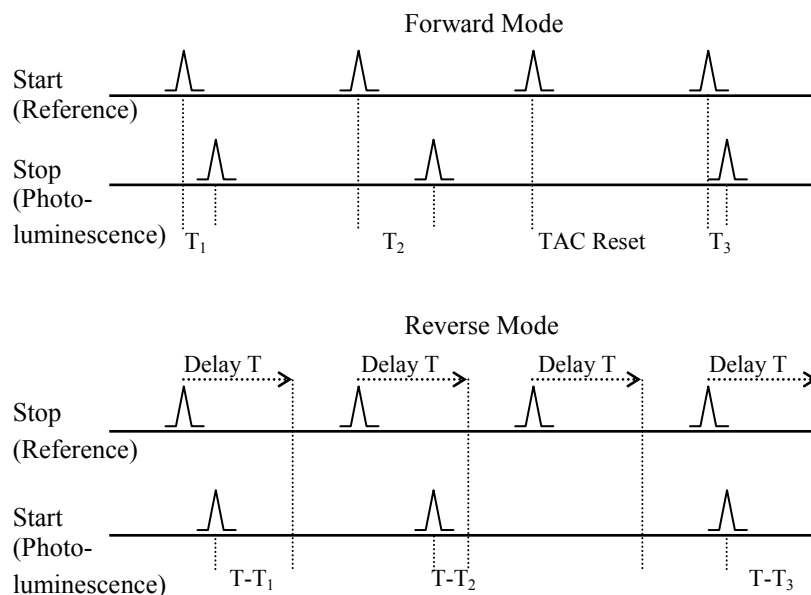
Figure A.2 In forward mode the TAC is initiated by every reference pulse and stopped by a signal pulse. In reverse mode the TAC is initiated only when a signal pulse is received, eliminating the need for TAC resets.

A.1.4 Constant Fraction Discriminator

Some adjustment of the constant fraction discriminator was necessary to obtain accurate measurements. The CFD settings for both the start and stop inputs can be found in the "CFD" tab of the "TCC900 Options" dialog box (see Fig. A.1(b)). Refer to section 2.6.2 for an explanation of the CFD's function.

The "Threshold" parameter determines how large an arriving pulse must be before it undergoes further processing. Pulses with an amplitude below the threshold level are ignored by the TCC900. Increasing the magnitude of this parameter will reduce the likelihood that random noise can trigger a start or stop event. The manual suggests a value that is 10% of the average pulse height. It is important to note that pulses from a photomultiplier tube can vary widely in height. Because of the uniformity of the reference pulses from the pulse generator we used a threshold value of -100 mV in the stop CFD. The start CFD threshold was typically -50 mV.

The temporal position of the pulse is determined by finding the steepest slope of the initial edge of the pulse. The "Fraction" and "Zero Crossing Level" parameters are used to optimize which portion of the slope is taken to be this steepest slope. Another parameter, the "Constant Fraction Delay," cannot be optimized by the software, but can be changed by inserting different delay circuits into the hardware of the TCC900 card itself. These TCSPC data did not appear to depend heavily on these parameters.. Adequate measurements were taken with a variety of settings including the suggested values of 20% fraction and -5 mV zero crossing level. Our measurements were typically taken with a 20% fraction and a -3 mV zero crossing level.

A.2   Ortec Model 9353 Fast Digitizer

The Ortec Model 9353 fast digitizer is much more simple to operate than the Edinburgh Instruments TCC900 card. With a 10 GHz internal clock, the card can be triggered at a rate of 82 MHz, and the inputs accept both positive and negative pulses. This means that there is no need for the pulse generator. There is also no option to run the Model 9353 in reverse mode.

This card was operated exclusively in "Time of Flight" (TOF) mode for our InGaAs QD measurements. This mode of operation is similar to the forward mode of the TCC900. See section 2.6.1 for greater explanation of this mode. The other mode of operation, "Chromat/Trend" mode, takes multiple TOF scans and tracks changes in the number of stop events over larger periods of time. This mode could be useful if, for example, the overall intensity of the signal was being modulated on a time scale much longer than the time of an individual TOF scan.

Like the TCC900, the measurement window for the Model 9353 has to be determined before the scan begins. This is done in the "Time of Flight mode" tab of the "Measurement Settings" dialog box. The time span field can accept a continuous range from 51.2 ns to 6.7 ms. Instead of choosing the number of bins, the user selects the desired time width of the bin with a minimum

resolution of 100 ps. For our solid QD scans we used a time span of 200 ns with a resolution of 100 ps. Extra reference pulses included in the 200 ns span were ignored by the Model 9353 and did not affect the measurement. The result was a time window that was triggered from the first start pulse and included as many as 17 excitation and decay cycles before resetting 200 ns later.

Because the Model 9353 does not use a constant fraction discriminator to determine the the temporal location of the incoming pulses, there are fewer settings to optimize. The Model 9353 allows the user to set the threshold levels on both the start and stop inputs as well as decide whether the input triggers on the falling edge or rising edge of the pulse. These values can be set automatically by the software using the "Auto Find" option, however, we typically set these levels manually for our experiments. Our measurements were taken with a stop threshold of -0.3 mV triggered on the falling edge and a start threshold of -0.34 mV triggered on the rising edge. These parameters are found in the "General" tab of the "Measurement Settings" dialog box.

Bibliography

[1] P. Bhattacharya, S. Ghosh, and A. Stiff-Roberts, "Quantum Dot Opto-Electronic Devices," Annu. Rev. Mater. Res. **34,** 1–40 (2004).

[2] H. Liu, M. Gao, J. McCaffrey, Z. Wasilewski, and S. Fafard, "Quantum Dot Infrared Photodetectors," Applied Physics Letters **78,** 79–81 (2001).

[3] V. Egorov, G. Cirlin, N. Polyakov, V. Petrov, A. Tonkikh, B. Volovik, Y. Musikhin, A. Zhukov, A. Tsatsulnikov, and V. Ustinov, "1.3-1.4 μm Photoluminescence Emission From InAs/GaAs Quantum Dot Multilayer Structures Grown on GaAs Singular and Vicinal Substrates," Nanotechnology **11,** 323–327 (2000).

[4] P. Anikeeva, J. Halpert, M. Bawendi, and V. Bulovic, "Quantum Dot Light-Emitting Devices with Electroluminescence Tunable over the Entire Visible Spectrum," Nano Letters **9,** 2532–2536 (2009).

[5] S. H. Pyun, S. H. Lee, and I. C. Lee, "Photoluminescence and lasing characteristics of InGaAs/InGaAsP/InP quantum dots," Journal of Applied Physics **96,** 5766–5770 (2004).

[6] K. Prabakar, S. Minkyu, and S. Inyoung, "CdSe quantum dots co-sensitized TiO2 photoelectrodes:particle size dependent properties," Journal of Physics D, Applied Physics **43,** 012002–1–012002–4 (2010).

[7] T. Campbell-Ricketts, N. A. J. M. Kleemans, and R. Notzel, "The role of dot height in determining exciton lifetimes in shallow InAs/GaAs quantum dots," Applied Physics Letters **96,** 033102–1 (2010).

[8] Y. I. Mazur, B. H. Liang, and Z. M. Wang, "Time-resolved photoluminescence spectroscopy of subwetting layer states in InGaAs/GaAs quantum dot structures," Journal of Applied Physics **100,** 054316–1–054316–5 (2006).

[9] C. Y. Ngo, S. F. Yoon, and D. R. Lim, "Temperature-dependent photoluminescence study of 1.3 mm undoped InAs/InGaAs/GaAs quantum dots," Applied Physics Letters **93,** 041912–041912 (2008).

[10] M. Syperek, P. Leszczynski, and J. Misiewicz, "Time-resolved photoluminescence spectroscopy of an InGaAs/GaAs quantum well-quantum dots tunnel injection structure," Applied Physics Letters **96,** 011901–1 (2010).

[11] S. Bose, "Quantum Communication through an Unmodulated Spin Chain," Physical Review Letters **91,** 1–4 (2003).

[12] W. Chang, T. Hsu, K. Tsai, T. Nee, J. Chyi, and N. Yeh, "Excitation Density and Temperature Dependent Photoluminescence of InGaAs Self-Assembled Quantum Dots," Japanese Journal of Applied Physics **38,** 554–557 (1999).

[13] D. Kim and H. Yang, "Shape Control of InGaAs Nanostructures on Nominal GaAs(001): Dashes and Dots," Nanotechnology **19,** 1–5 (2008).

[14] J. Lee, Z. Wang, B. Liang, W. Black, V. Kunets, Y. Mazur, and G. Salamo, "Selective Growth of InGaAs/GaAs Quantum Dot Chains on Pre-Patterned GaAs(001)," Nanotechnology **17,** 2275–2278 (2006).

[15] V. Turck, F. Heinrichsdorff, M. Veit, R. Heitz, M. Grundmann, A. Krost, and D. Bimberg, "Correlation of InGaAs/GaAs Quantum Dot and Wetting Layer Formation," Applied Surface Science **123,** 352–355 (1998).

[16] Z. Wang, K. Holmes, Y. Mazur, and G. Salamo, "Fabrication of (In,Ga)As Quantum-Dot Chains on GaAs(100)," Applied Physics Letters **84,** 1931–1933 (2004).

[17] G. Slepyan, Y. Yerchak, A. Hoffman, and F. Bass, "Strong Electron-Photon Coupling in a On-Dimensional Quantum Dot Chain: Rabi Waves and Rabi Wave Packets," Physical Review B **81,** 1–18 (2010).

[18] S. Mirabella, R. Agosta, G. Franzo, I. Crupi, M. Miritello, R. L. Savio, M. D. Stefano, S. D. Marco, and A. Terrasi, "Light Absorption in Silicon Quantum Dots Embedded in Silica," Journal of Applied Physics **106,** 103505–1–103505–8 (2010).

[19] A. Jones, "Photoluminescence of Indium Gallium Arsenide Quantum Dots and Dot Chains," Brigham Young University Thesis (2010).

[20] Y. I. Mazur, B. H. Liang, Z. M. Wang, G. Tasarov, D. Guzun, and G. Salamo, "Lengthening of the Photoluminescence Decay Time of InAs Quantum Dots Coupled to InGaAs/GaAs Quantum Well," Journal of Applied Physics **100,** 054313–1–054313–4 (2006).